Theor Chem Acc (2009) 124:269–278
DOI 10.1007/s00214-009-0607-z

REGULAR ARTICLE

First-principles determination of molecular conformations of indolizidine (−)-235B′ in solution

Fang Zheng · Linda P. Dwoskin · Peter A. Crooks · Chang-Guo Zhan

Received: 12 June 2009 / Accepted: 9 July 2009 / Published online: 28 July 2009

Abstract Indolizidine (−)-235B′ is a particularly interesting natural product, as it is the currently known, most potent and subtype-selective open-channel blocker of the $\alpha4\beta2$ nicotinic acetylcholine receptor (nAChR). In the current study, extensive first-principles electronic structure calculations have been carried out in order to determine the stable molecular conformations and their relative free energies of the protonated and deprotonated states of (−)-235B′ in the gas phase, in chloroform, and in aqueous solution. The ^{1}H and ^{13}C NMR chemical shifts calculated using the computationally determined dominant molecular conformation of the deprotonated state are all consistent with available experimental NMR spectra of (−)-235B′ in chloroform, which suggests that the computationally determined molecular conformations are reasonable. Our computational results reveal for the first time that two geminal H atoms on carbon-3 (C3) of (−)-235B′ have remarkably different chemical shifts (i.e., 3.24 and 2.03 ppm). The computational results help one to better understand and analyze the experimental ^{1}H NMR spectra of (−)-235B′. The finding of remarkably different chemical shifts of two C3 geminal H atoms in a certain molecular conformation of (−)-235B′ may also be valuable in analysis of NMR spectra of other related ring-containing compounds. In addition, the pK_a of (−)-235B′ in aqueous solution is predicted to be ∼9.7. All of the computational results provide a solid basis for future studies of the microscopic and phenomenological binding of various receptor proteins with the protonated and deprotonated structures of this unique open-channel blocker of $\alpha4\beta2$ nAChRs. This computational study also demonstrates how one can appropriately use computational modeling and spectroscopic analysis to address the structural and spectroscopic problems that cannot be addressed by experiments alone.

Keywords Molecular conformation · Antagonist of receptor protein · Blocker of ion channel · NMR chemical shift

1 Introduction

Natural products exhibit a remarkable diversity of structural motifs that can be systematically exploited for drug discovery [1]. Thus, natural products provide one of the richest sources of scaffold structures for the identification of novel leads for rational drug design. Alkaloids detected in amphibian skin contain over 20 structural classes, in which various biologically active, lipid-soluble alkaloids have been discovered [2]. Besides the epibatidines that are leads in the drug design of new analgesics [3, 4], the largest subclass of these alkaloids, i.e., the 5,8-disubstituted indolizidines, has attracted much interest [5].

So far, about 80 entities of 5,8-disubstituted indolizidines have been found in skin extracts from frogs and toads [2]. None of these alkaloids have been identified from any other natural source. Many research groups across the world have expended great effort into the synthesis [5–8], and characterization of such compounds [9, 10]. The 5,8-disubstituted indolizidine alkaloid, (−)-235B′ (Fig. 1, the C numbering system is taken from Edwards and Daly [11]) isolated from *Dendrobates pumilio* (the poison dart frog), is one of the well-characterized ligands of nicotinic

F. Zheng · L. P. Dwoskin · P. A. Crooks · C.-G. Zhan (✉)
Department of Pharmaceutical Sciences,
College of Pharmacy, University of Kentucky,
725 Rose Street, Lexington, KY 40536, USA
e-mail: zhan@uky.edu

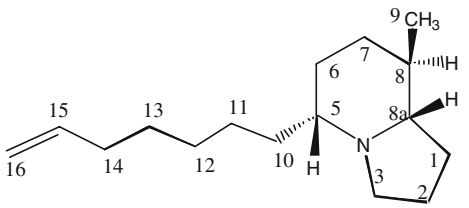

Fig. 1 Molecular structure of (−)-235B′

acetylcholine receptors (nAChRs). Unlike epibatidine, which is a potent agonist of $\alpha4\beta2$ nAChRs [3], (−)-235B′ acts as a noncompetitive and subtype-selective antagonist of $\alpha4\beta2$ nAChRs [10]. Neuronal nAChRs are members of a superfamily of ligand-gated ion channels, which modulate the function of many major neurotransmitter systems and influence a broad range of brain functions, including cognition, learning, and memory [12–16]. Selective $\alpha4\beta2$ nAChR agonists and antagonists have therapeutic potential in the treatment of Alzheimer's disease [17], Parkinson's disease [18], pain [19], and tobacco-use addiction, etc. [20]. (−)-235B′ is currently the most potent and subtype-selective open-channel blocker ($IC_{50} = 74$ nM) of $\alpha4\beta2$ nAChRs. This noncompetitive antagonist of $\alpha4\beta2$ nAChRs is being considered as a promising lead for new drug discovery to treat cholinergic disorders such as autosomal dominant nocturnal frontal lobe epilepsy [9, 10], and to treat smoke addiction in our study.

The particular characteristics of (−)-235B′ indicate that understanding how this alkaloid interacts with neuronal nAChRs may aid in the rational drug design of more potent antagonists that alter nicotine cholinergic functions in a subtype-selective manner. In addition to quantitative structure–activity relationship (QSAR) studies [21–23], molecular modeling and simulation of nAChR binding with agonists and antagonists have provided a better understanding of the molecular mechanisms involved in nAChR function, in addition to results obtained using [^{3}H]nicotine binding assays, electrophysiology, and molecular biology [24]. As demonstrated in our previous computational studies on other nAChR ligands [25–28], in order to study how a ligand binds with an nAChR, we first need to know various possible molecular structures and conformations of the ligand itself. This is because an alkaloid, such as (−)-235B′, can exist in multiple possible molecular species (protonated and deprotonated states) in aqueous solution. Furthermore, for a given protonation state, the ligand could also exist in various possible molecular conformations. All of the possible protonation states/conformations could bind to a receptor protein with different binding affinities. It has been demonstrated in our previous computational studies [25] on nicotine and deschloroepibatidine that the most stable molecular species and conformer in solution is not necessarily the most important molecular species and conformer that interacts with the binding site of an nAChR. Therefore, all molecular species of (−)-235B′, whether protonated or deprotonated, and all the possible conformations are potentially important for binding with the protein when the differences between the relative concentrations of different molecular species and conformations of the free ligand in solution are not very large. The relative Gibbs free energies of different molecular species and conformations are important information required to determine their concentration distribution in solution and their relative contributions to the receptor-ligand binding. In order to determine the phenomenological binding free energy, one must know both the relative free energies of various molecular species/conformations of the free ligand in solution and the microscopic binding free energies associated with all molecular species/conformations. Knowing the concentration distribution of all structural forms of (−)-235B′ in solution, one can further study the theoretical binding of each structural form with the nAChR and evaluate the microscopic binding free energy. The appropriately combined use of the calculated microscopic binding free energies and the concentration distribution of different structural forms of (−)-235B′ can then lead to a theoretical prediction of the overall, phenomenological binding free energy for (−)-235B′ binding with the nAChR, as demonstrated in our recent computational studies on other nAChR ligands [25, 26, 28].

With a goal to eventually understand the microscopic and phenomenological binding of frog toxin (−)-235B′ with $\alpha4\beta2$ and many other nAChRs, as well as the open-channel blocking effects of this ligand on the acetylcholine-activated $\alpha4\beta2$ nAChRs in electrophysiological measurements, in the present study we carefully examined various possible molecular conformations of both the protonated and deprotonated states of (−)-235B′ and predicted their ^{1}H and ^{13}C nuclear magnetic resonance (NMR) chemical shifts and relative Gibbs free energies in solution by carrying out extensive first-principles electronic structure calculations that accurately account for solvent effects. The calculated results and analysis have led us to better understand the detailed molecular structures and NMR spectra of (−)-235B′ in solution.

2 Results and discussion

2.1 Optimized geometries and calculated relative free energies

We first carried out a detailed conformational search for various possible conformations of the neutral (deprotonated) state of (−)-235B′. The conformational search was

focused on various possible conformations of the rings, with the understanding that the seven-carbon chain external to the bicyclic portion should exist in the all-anti conformation. Depicted in Fig. 2 are four stable conformations that were identified: two chair conformations, denoted by (−)-235B′-A and (−)-235B′-B, and two boat conformations, denoted by (−)-235B′-C and (−)-235B′-D. The geometry optimization starting from any one of the initial structures considered in this study eventually went to one of these four stable geometries, or to an unstable geometry with at least one imaginary vibrational frequency. The relative Gibbs free energies calculated for these deprotonated conformers in the gas phase and in solution (i.e., chloroform and aqueous solution) are summarized in Table 1.

As one can see from Table 1, the energetic results calculated in the gas phase and in solution using two different solvation models and various basis sets are all qualitatively consistent with each other. Particularly, the calculated relative free energies are not sensitive to the basis set used in the calculations. When the same solvation method was used, the differences between the B3LYP/6-31+G(d) results and the corresponding 6-31++G(d,p) results are only about 0.1 or 0.2 kcal/mol. Further increasing the basis set from 6-31++G(d,p) to 6-311++G(d,p) and to 6-311++G(2d,2p), the changes of the calculated relative free energies are all within 0.2 kcal/mol. The consistent energetic results suggest that even 6-31+G(d), the smallest one of the four basis sets examined in this study, is adequate for studying the relative stability of the various conformations involved in this work. For convenience, unless otherwise indicated, the discussion below will only refer to the energetic results associated with the SVPE solvation model and the largest one of the four basis sets, i.e., 6-311++G(2d,2p).

Table 1 Calculated relative Gibbs free energies (ΔG in kcal/mol) of the conformations of the deprotonated state of (−)-235B′ in the gas phase (298.15 K and 1 atm) and in solution

Computational method[a]	Conformation of (−)-235B′			
	A	B	C	D
ΔG in the gas phase				
6-31+G(d)	0	12.2	6.5	10.2
6-31++G(d,p)	0	12.0	6.4	10.1
6-311++G(d,p)	0	11.8	6.3	9.9
6-311++G(2d,2p)	0	11.9	6.3	10.1
ΔG in chloroform solution				
6-31+G(d) + SVPE	0	11.9	6.6	10.5
6-31++G(d,p) + SVPE	0	11.7	6.5	10.4
6-311++G(d,p) + SVPE	0	11.5	6.3	10.2
6-311++G(2d,2p) + SVPE	0	11.6	6.3	10.4
6-311++G(d,p) + IEFPCM	0	12.0	6.9	10.5
ΔG in aqueous solution				
6-31+G(d) + SVPE	0	11.8	6.6	10.7
6-31++G(d,p) + SVPE	0	11.6	6.5	10.6
6-311++G(d,p) + SVPE	0	11.4	6.4	10.4
6-311++G(2d,2p) + SVPE	0	11.4	6.4	10.6

[a] The gas phase free energies were calculated by using the B3LYP functional and various basis sets with the zero-point and thermal corrections at the B3LYP/6-31+G(d) level. The solvent shifts were calculated by using either the SVPE or IEFPCM method

The energetic results in Table 1 reveal that the most stable conformation of the deprotonated state is always (−)-235B′-A, no matter whether it is in the gas phase, in chloroform, or in aqueous solution. The free energies of the other conformations are higher than that of (−)-235B′-A by ∼6.3 to 11.9 kcal/mol in the gas phase, by ∼6.9 to 12.0 kcal/mol in chloroform, and by ∼6.4 to 11.4 kcal/mol in aqueous

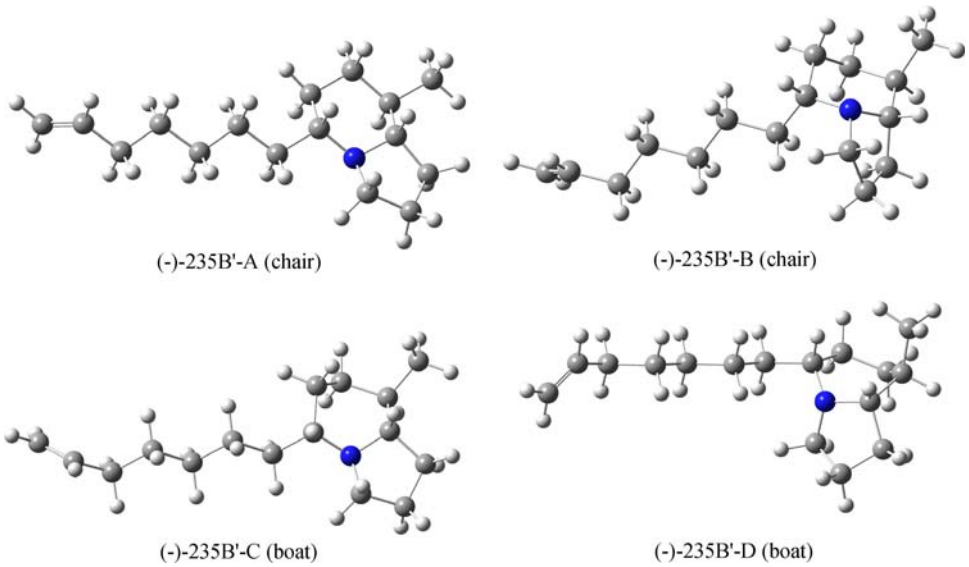

Fig. 2 Stable conformations of the deprotonated state of (−)-235B′ optimized at the B3LYP/6-31+G(d) level

solution. Based on the calculated relative free energies, (−)-235B′-A should always be the dominant conformation of the deprotonated state both in the gas phase, in chloroform, and in aqueous solution. For example, the calculated free energy difference of ∼6.9 kcal/mol between (−)-235B′-A and (−)-235B′-C in chloroform suggests that the ratio of the concentration of (−)-235B′-A to that of (−)-235B′-C is $\sim 1.1 \times 10^5$ at room temperature (298.15 K).

Starting from the optimized geometries of the deprotonated state, geometries of the corresponding conformations in the protonated state were optimized. Depicted in Fig. 3 are the optimized geometries: (−)-235B′H^+-A, (−)-235B′H^+-B, (−)-235B′H^+-C, and (−)-235B′H^+-D, which are the protonated structures of (−)-235B′-A, (−)-235B′-B, (−)-235B′-C, and (−)-235B′-D, respectively. The calculated relative free energies are summarized in Table 2. As shown in Table 2, the calculated relative free energies are also insensitive to the basis set used in the calculations. The differences between the B3LYP/6-31+G(d) results and the 6-31++G(d,p) results are about 0.1 or 0.2 kcal/mol. The differences between the B3LYP/6-31++G(d,p) results and the 6-311++G(d,p) results are between 0.0 and 0.2 kcal/mol. Further increasing the basis set from 6-311++G(d,p) and to 6-311++G(2d,2p), the changes of the calculated relative free energies are all within 0.1 kcal/mol. The discussion below will only refer to the energetic results calculated at the B3LYP/6-311++G(2d,2p) level.

As seen in Table 2, the relative free energies of the four conformations of the protonated state of (−)-235B′ are qualitatively the same as those of the corresponding four conformations of the deprotonated state. The most stable conformation of the protonated state is (−)-235B′H^+-A in both the gas phase and in aqueous solution. We did not calculate the protonated state in chloroform solution because the experimental NMR spectra were available only for the free base (i.e., the deprotonated state) of (−)-235B′ in chloroform solution. The free base of (−)-235B′ is not expected to be protonated in chloroform solution. The free energies of the other conformations are higher than that of (−)-235B′H^+-A by ∼6.4 to 10.3 kcal/mol in the gas phase and ∼6.9 to 9.7 kcal/mol in aqueous solution. Protonation slightly decreases the differences in free energy between the most stable conformation and the others. The calculated free energy difference of ∼6.9 kcal/mol between (−)-235B′H^+-A and (−)-235B′H^+-C in aqueous solution

Table 2 Calculated relative Gibbs free energies (ΔG in kcal/mol) of the conformations of the protonated state of (−)-235B′ in the gas phase (298.15 K and 1 atm) and in solution

Computational method[a]	Conformation of (−)-235B′H^+			
	A	B	C	D
ΔG in the gas phase				
6-31+G(d)	0	10.7	6.6	8.3
6-31++G(d,p)	0	10.5	6.5	8.1
6-311++G(d,p)	0	10.3	6.5	8.0
6-311++G(2d,2p)	0	10.3	6.4	8.1
ΔG in aqueous solution				
6-31+G(d)+SVPE	0	10.1	7.1	9.5
6-31++G(d,p)+SVPE	0	9.9	7.0	9.3
6-311++G(d,p)+SVPE	0	9.7	7.0	9.2
6-311++G(2d,2p)+SVPE	0	9.7	6.9	9.3

[a] The gas phase free energies were calculated by using the B3LYP functional and various basis sets with the zero-point and thermal corrections at the B3LYP/6-31+G(d) level. The solvent shifts were calculated by using either the SVPE or IEFPCM method

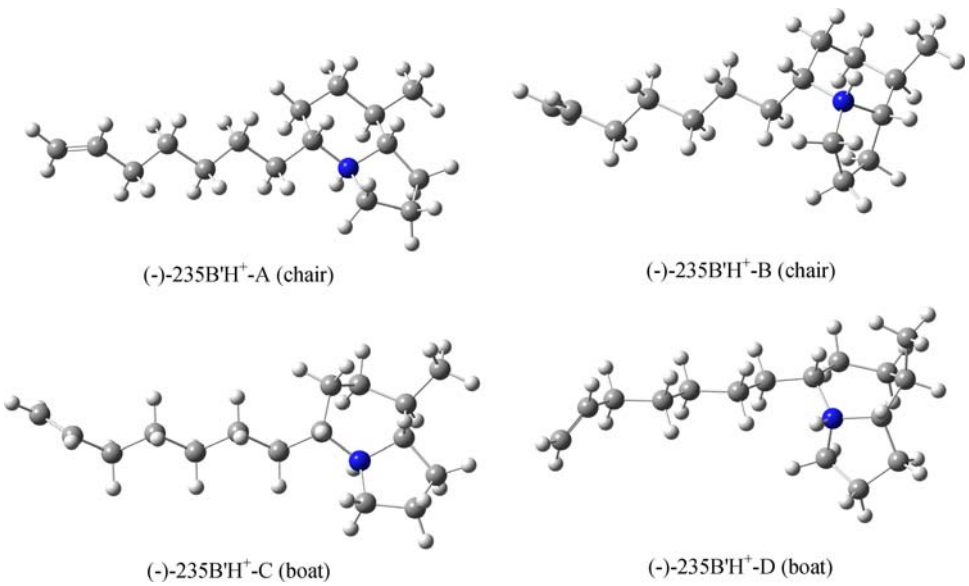

Fig. 3 Stable conformations of the protonated state of (−)-235B′, denoted by (−)-235B′H^+, optimized at the B3LYP/6-31+G(d) level

predicts that the ratio of the concentration of (−)-235B′H$^+$-A to that of (−)-235B′H$^+$-C is $\sim 1.1 \times 10^5$ at 298.15 K.

2.2 NMR chemical shifts

Witala, Cramer, and Hoye recently used computed ^{1}H and ^{13}C NMR chemical shifts to distinguish stereoisomers of diastereomeric penam beta-lactams [29]. In order to compare the optimized geometries with available experimental structural information (i.e., ^{1}H and ^{13}C NMR spectra in chloroform) [30, 31] on this nAChR antagonist, we calculated the ^{1}H and ^{13}C NMR chemical shifts for each of the optimized geometries of the deprotonated state in chloroform. The predicted ^{1}H and ^{13}C NMR chemical shifts are summarized in Tables 3 and 4 in comparison with the available experimental data [30, 31]. It should be pointed out that an alkaloid such as (−)-235B′ in chloroform solution can only exist in the deprotonated state, although the protonated state could be dominant in aqueous solution. Thus, the experimental NMR chemical shifts [30] should be compared to the results calculated for the deprotonated state. The assignment of the experimental NMR chemical shifts is based on the chemical shifts calculated for (−)-235B′-A, since this should be the dominant conformation, as discussed above.

The computational results summarized in Table 3 show a remarkable difference in the pattern of the distribution of the calculated ^{1}H NMR chemical shifts between conformations (−)-235B′-A and (−)-235B′-C, and conformations (−)-235B′-B and (−)-235B′-D. In particular, in (−)-235B′-B and (−)-235B′-D, there are four H atoms with ^{1}H NMR chemical shifts between 2.7 and 3.3 ppm, whereas in (−)-235B′-A and (−)-235B′-C, there is only one H atom with a chemical shift between $\sim$2.3 and $\sim$4.8 ppm. Only the patterns corresponding to (−)-235B′-A and (−)-235B′-C are consistent with the available ^{1}H NMR spectra[30] (see Table 3 for the experimental ^{1}H NMR chemical shifts). As seen in Table 3, only one H atom has a chemical shift (3.25 ppm) between $\sim$2.3 and $\sim$4.8 ppm. Thus, based on the patterns for the distribution of the calculated ^{1}H NMR chemical shifts, conformations (−)-235B′-B and (−)-235B′-D can be excluded as being present in chloroform solution. However, both (−)-235B′-A (chair) and (−)-235B′-C (boat) conformations are possible.

In both (−)-235B′-A and (−)-235B′-C, a unique H atom with a chemical shift between $\sim$2.3 and $\sim$4.8 ppm, i.e., one of the two H atoms on C3 (see Fig. 1), is observed. The chemical shift of H^a-3 is predicted to be 3.24 ppm in (−)-235B′-A and 3.23 ppm in (−)-235B′-C, and all are very close to the experimental chemical shift of 3.25 ppm[30] or 3.23 ppm [31]. The chemical shift of the other H atom (H^b-3) on C3 is predicted to be 2.03 ppm in (−)-235B′-A and 1.89 ppm in (−)-235B′-C, and all are close to the observed chemical shift of 1.80–1.97 ppm [30]. The computational results clearly predict that the chemical shifts of the two geminal H atoms on C3 are considerably different, with a remarkable difference of 1.21 ppm in the (−)-235B′-A (chair) conformer and 1.34 ppm in the (−)-235B′-C (boat) conformer. This implies that the two geminal H atoms on C3 in these two conformations experience remarkably different chemical environments/magnetic shielding such that they have remarkably different chemical shifts. With this point in mind, it is not surprising to note that the difference in the chemical shift between the two geminal H atoms on C3 is dependent on the conformation of the molecule. As seen in Table 3, in the (−)-235B′-B (chair) or (−)-235B′-D (boat) conformer, the difference between the calculated chemical shifts of the two geminal H atoms on C3 is negligible (0.02 or 0.05 ppm).

The calculated ^{1}H NMR chemical shifts can help us to better understand and correctly analyze the experimental ^{1}H NMR spectra. The experimental ^{1}H NMR chemical shifts were assigned by Collins et al. [31]. It is notable that Collins et al. [31] assigned the chemical shift at 3.23 ppm to the H atom on C8a. This assignment is not supported by our computational data, since the calculated chemical shift of H-8a is only $\sim$1.55 ppm. It is more reasonable to assign the chemical shift at 3.23 ppm [31] (or 3.25 ppm in another experimental measurement [30]) to one of the H atoms on C3, based on the aforementioned discussion. Except for the chemical shifts of the H atoms on C3 and C8a, the assignments by Collins et al. for all the other ^{1}H chemical shifts (i.e., at 5.77, 4.95, 2.89, 2.00, 0.86–1.95, and 0.83 ppm) [31] are supported by our calculated results. It should be pointed out that the relative magnitudes of our calculated chemical shifts (1.10, 0.84, and 0.59 ppm) for the three H atoms on C9 are significantly different from those of the chemical shifts observed for these three H atoms (all at 0.83 ppm). This is because our NMR calculations were carried out on a single conformation of the structure (local minimum). Practically, any molecule will undergo thermal motions. The methyl group (consisting of C9 and its attached three H atoms) of (−)-235B′ can easily rotate during the experimental process, so that the three H atoms are statistically equivalent, unlike the two non-rotatable geminal H atoms on C3. Thus, the experimentally observed ^{1}H NMR chemical shifts of the three H atoms of the methyl group should reflect the statistical average of the chemical shifts of the three rotatable H atoms. Consequently, it is better to compare the average value of the calculated three ^{1}H chemical shifts with the experimental chemical shift for the three H atoms of the methyl group. The average value of the calculated chemical shifts of the three H atoms is $(1.10 + 0.84 + 0.59)/3 = 0.84$ ppm, which is very close to the experimental values of 0.83 ppm [31] or 0.85 ppm [30].

Table 3 ^{1}H NMR chemical shifts (δ_H in ppm) of (−)-235B′ in chloroform calculated by using the GIAO method at the IEFPCM-B3LYP/6-311 ++G(d,p) level in comparison with available experimental data

H atom, see Fig. 1	Calc. δ_H for (−)-235B′-D	Calc. δ_H for (−)-235B′-C	Calc. δ_H for (−)-235B′-B	Calc. δ_H for (−)-235B′-A	Expt. δ_H in $CDCl_3$ (500 MHz)[a]	Expt. δ_H in $CDCl_3$ (400 MHz)[b]
H-15	6.34	6.38	6.42	6.39	5.80	5.77
H^a-16	5.32	5.31	5.34	5.29	4.98	4.95
H^b-16	5.16	5.16	5.15	5.17	4.92	4.89
H^a-3	2.83	3.23	2.94	3.24	3.25	3.23
H^a-14	2.15	2.21	2.21	2.22	2.03	2.00
H^b-14	1.97	2.04	2.05	2.03	2.03	2.00
H^b-3	2.78	1.89	2.92	2.03	1.80–1.97	0.86–1.95
H-5	2.97	2.21	2.83	1.89	1.80–1.97	0.86–1.95
H^a-1	2.24	1.96	1.62	1.83	1.80–1.97	0.86–1.95
H^a-2	1.78	1.78	1.62	1.73	1.80–1.97	0.86–1.95
H^a-6	1.49	1.63	1.79	1.73	1.58–1.77	0.86–1.95
H^a-7	1.70	2.04	1.10	1.64	1.58–1.77	0.86–1.95
H^a-10	1.38	1.46	1.33	1.64	1.58–1.77	0.86–1.95
H-8[a]	3.30	1.96	2.68	1.55	1.58–1.77	0.86–1.95
H^a-13	1.43	1.46	1.46	1.55	1.58–1.77	0.86–1.95
H^b-2	1.68	1.63	1.62	1.55	1.16–1.50	0.86–1.95
H^a-11	1.67	1.31	0.98	1.40	1.16–1.50	0.86–1.95
H^b-1	1.47	1.31	1.33	1.40	1.16–1.50	0.86–1.95
H-8	1.38	1.63	1.96	1.30	1.16–1.50	0.86–1.95
H^a-12	1.34	1.31	1.33	1.30	1.16–1.50	0.86–1.95
H^b-12	1.28	1.32	1.33	1.30	1.16–1.50	0.86–1.95
H^b-13	1.19	1.21	1.17	1.19	1.16–1.50	0.86–1.95
H^b-6	1.47	1.31	1.46	1.10	1.16–1.50	0.86–1.95
H^b-10	1.29	1.31	1.33	1.10	1.16–1.50	0.86–1.95
H^b-11	1.17	1.21	1.33	1.10	1.16–1.50	0.86–1.95
H^b-7	1.39	0.88	1.86	1.01	0.94	0.86–1.95
H^a-9	1.40	0.99	1.79	1.10	0.85	0.83
H^b-9	0.96	0.99	0.98	0.84	0.85	0.83
H^c-9	0.96	0.88	0.79	0.59	0.85	0.83
r^2 [c]	0.898	0.985	0.889	0.989	NA	NA
RMSD (ppm)[c]	0.39	0.15	0.41	0.13	NA	NA

[a] Experimental data from Ref. [30]

[b] Experimental data from Ref. [31]

[c] Correlation constant (r^2) and root-mean-square deviation (RMSD) for the linear regression analysis between the calculated and experimental ^{1}H NMR chemical shifts (500 MHz, Ref. [30]). For the experimental chemical shifts given by a range, the middle value of the range was used in the linear regression analysis

Further, we examined the linear correlation between the calculated and experimental ^{1}H NMR chemical shifts. The obtained values of the correlation constant (r^2) and root-mean-square deviation (RMSD) are also summarized in the last two rows of Table 3. As seen in Table 3, the linear correlation between the calculated and experimental ^{1}H NMR chemical shifts for (−)-235B′-A (chair) and (−)-235B′-C (boat) is significantly better than that for (−)-235B′-B (chair) and (−)-235B′-D (boat). The best linear correlation is associated with (−)-235B′-A (chair).

The predicted ^{13}C NMR chemical shifts are summarized in Table 4. The patterns for the distribution of the ^{13}C NMR chemical shifts calculated for all the conformations of the deprotonated state are reasonably close to that of the experimental ^{13}C NMR chemical shifts [30]. A comparison of the ^{13}C NMR chemical shifts still does not allow one to distinguish whether the experimentally observed conformation should be (−)-235B′-A (chair) or (−)-235B′-C (boat). We also examined the linear correlation between the calculated and experimental ^{13}C NMR chemical shifts.

Table 4 ^{13}C NMR chemical shifts (δ_C in ppm) of (−)-235B′ in chloroform calculated by using the GIAO method at the IEFPCM-B3LYP/6-311++G(d,p) level in comparison with available experimental data

H atom, see Fig. 1	Calc. δ_C for (−)-235B′-D	Calc. δ_C for (−)-235B′-C	Calc. δ_C for (−)-235B′-B	Calc. δ_C for (−)-235B′-A	Expt. δ_C in $CDCl_3$ (125 MHz)[a]
C15	153.06	152.68	152.46	152.73	139.14
C16	119.41	118.87	118.94	118.59	114.16
C8a	69.91	70.60	70.34	76.16	71.31
C5	56.59	66.90	64.06	68.32	63.49
C3	49.94	58.10	56.52	56.01	51.83
C8	40.42	44.20	33.78	43.89	36.56
C14	42.34	42.62	42.71	42.49	34.56
C10	41.53	39.20	36.33	40.99	33.74
C7	26.58	29.28	24.35	38.57	33.68
C13	38.39	38.18	37.87	37.92	31.22
C12	37.58	37.62	37.87	37.92	29.53
C6	28.21	26.71	25.41	36.33	29.04
C1	39.63	34.94	36.62	34.19	28.87
C11	34.79	33.92	34.98	32.97	25.66
C2	30.62	26.82	29.76	24.67	20.33
C9	23.22	21.32	23.77	20.76	18.88
r^2 [b]	0.969	0.986	0.974	0.996	N.A.
RMSD (ppm)[b]	5.89	3.99	5.71	2.23	N.A.

[a] Experimental data from Ref. [30]

[b] Correlation constant (r^2) and root-mean-square deviation (RMSD) for the linear regression analysis between the calculated and experimental ^{13}C NMR chemical shifts (Ref. 30)

The obtained r^2 and RMSD values are summarized in the last two rows of Table 4. Data summarized in Table 4 show that the linear correlation between the calculated and experimental ^{13}C NMR chemical shifts for (−)-235B′-A (chair) and (−)-235B′-C (boat) is significantly better than that for (−)-235B′-B (chair) and (−)-235B′-D (boat). The best linear correlation is also associated with (−)-235B′-A (chair).

In summary, the comparison in both ^{1}H and ^{13}C NMR spectra between the computational results and experimental data cannot conclusively determine whether the experimentally observed conformation should be (−)-235B′-A (chair) or (−)-235B′-C (boat). These two conformations must be distinguished by use of the predicted relative free energies (discussed above). The calculated relative free energies show that the experimentally observed conformation should be (−)-235B′-A (chair), rather than (−)-235B′-C (boat). It is especially interesting to note that the computationally predicted ^{1}H NMR chemical shifts for the two C3 geminal hydrogen atoms of (−)-235B′ in the most stable conformation are remarkably different, which helps to better understand the experimental ^{1}H NMR spectra reported in the literature. As shown in Tables 3 and 4, the ^{1}H and ^{13}C NMR chemical shifts calculated for (−)-235B′-A are all reasonably close to the corresponding experimental data [30], according to the detailed assignments summarized in the tables.

2.3 Energetics and pK_a

In addition to the determination of dominant molecular conformations, it is also interesting to predict the pK_a of (−)-235B′ in aqueous solution to eventually understand the microscopic and phenomenological binding of the receptor protein with the protonated and deprotonated structures of this important open-channel blocker of $\alpha4\beta2$ nAChRs. Knowing the pK_a value will allow evaluation of the relative concentrations of the protonated and deprotonated states at any pH. The pK_a of (−)-235B′ is determined by the Gibbs free energy change in aqueous solution (ΔG_a) of the following protonation process:

$$(-)\text{-}235\text{B}'\text{H}^+ \rightarrow (-)\text{-}235\text{B}' + \text{H}^+ \quad (1)$$

The pK_a can be evaluated via

$$\text{p}K_a = \Delta G_a/(2.303RT). \quad (2)$$

Prediction of the free energy change of a deprotonation process requires knowing the absolute free energy of the proton (H^+) in aqueous solution, $\Delta G^{298}_{hyd}(H^+)$, in addition to the free energies calculated for all of the molecular species (i.e., protonated and deprotonated states) discussed above. Due to the inherent difficulty of measuring absolute solvation free energy of an ion, the reported "experimental" $\Delta G^{298}_{hyd}(H^+)$ values have a wide range from −252.6 to −264.1 kcal/mol [32]. We predicted $\Delta G^{298}_{hyd}(H^+)$(by using a high-level, ab initio method of

incorporating a hybrid supermolecule-continuum approach based on the same SVPE procedure used in the present study) to be −262.4 kcal/mol [33]. The same computational protocol has been used to calculate the pK_a for cocaine, nicotine, and other organic amines, and the calculated pK_a values are all in good agreement with the corresponding experimental data. Thus, the pK_a of (−)-235B′ in aqueous solution was calculated to be ∼9.7 in the present study. The calculated pK_a value of ∼9.7 predicts that the concentration of the protonated state of (−)-235B′ should be higher than that of the deprotonated state when the pH < ∼9.7, but the concentration of the deprotonated state of (−)-235B′ should be higher than that of the protonated state when the pH >9.7. Particularly, in aqueous solution at a physiological pH (7.4), ∼99.5% of (−)-235B′ should exist in the (−)-235B′H$^+$-A conformer, while only ∼0.5% of (−)-235B′ should exist in the (−)-235B′-A conformer. The other conformations (B to D) are negligible for both the protonated and deprotonated states in aqueous solutions. Further computational studies on (−)-235B′ binding with nAChRs may be focused on the (−)-235B′H$^+$-A conformer of the protonated species and the (−)-235B′-A conformer of the deprotonated species.

2.4 Computational methods

In order to search for stable molecular geometries, we first needed to build various possible initial structures of (−)-235B′. The initial structures of the deprotonated state used in the geometry optimizations were built in consideration of various possible chair and boat conformations. Geometries of all structures considered in this study were optimized by using gradient-corrected density functional theory (DFT) with the B3LYP functional [34–36] and 6-31+G(d) basis set [37]. The optimized geometries were used to carry out the harmonic frequency analysis at the same B3LYP/6-31+G(d) level, to make sure that each of the optimized geometries is associated with a local minimum on the potential energy surface, and to evaluate the zero-point and thermodynamic corrections to the Gibbs free energy. The geometries optimized at the B3LYP/6-31+G(d) level were also used to carry out single-point energy calculations using larger basis sets at the B3LYP/6-31++G(d,p), B3LYP/6-311++G(d,p), and B3LYP/6-311++G(2d,2p), levels, in order to make sure that the basis set used in this study is adequate.

The geometries optimized at the B3LYP/6-31+G(d) level were also used to perform self-consistent reaction field (SCRF) energy calculations in aqueous solution, in order to determine the solvent shifts. Florian and Warshel [38] performed a manual geometry search in solution along the corresponding gas phase intrinsic reaction coordinate for the hydrolysis of mono-methyl phosphate, and demonstrated that the contributions of the solvent-induced structural changes to the overall energetics are small and can be safely neglected. The calculated free energies in aqueous solution were taken as the energies calculated in the gas phase with the B3LYP/6-31+G(d) zero-point and thermal corrections (at 298 K and 1 atm) plus the corresponding solvent shifts determined by the SCRF calculations. The main SCRF method used in this study for the energy calculations is known as the surface and volume polarizations for electrostatics (SVPE) [39–42]. This SVPE method is also known as the fully polarizable continuum model (FPCM) [25, 43–56], because it fully accounts for both surface and volume polarization effects on the solute–solvent electrostatic interaction. The SVPE method, which was initially developed in the GAMESS program [57] by one of us (Zhan) with Chipman and Bentley [39], has been implemented recently in our local version [58] of the Gaussian03 program [59]. Some advantages of the SVPE method over other SCRF methods can be found in our previous reports concerning reaction field calculations using various SCRF methods on the energy barriers of a series of carboxylic acid esters [42] and phosphate esters, including a simplified cAMP model [60]. The SVPE calculations in solvent water (with dielectric constant $\varepsilon = 78.304$) or chloroform ($\varepsilon = 4.9$) were carried out at the HF/6-31+G* level, as it has been shown [61] that electron correlation does not significantly affect the calculated solvent shifts.

In addition, we also employed the geometries optimized at the B3LYP/6-31+G(d) level to carry out nuclear magnetic shielding calculations at the B3LYP/6-311++G(d,p) level using the gauge-independent atomic orbital (GIAO) method [62–65] in combination with the integral equation formalism of the polarizable continuum model (IEFPCM) [66–72] implemented in the Gaussian03 program [59]. The IEFPCM method used in the GIAO calculations accounted for the effects of solvent chloroform ($\varepsilon = 4.9$) on the nuclear magnetic shielding tensors, as experimental NMR spectra available for (−)-235B′ were measured in chloroform. In order to determine the isotropic ^{1}H and ^{13}C NMR chemical shifts, we also carried out the GIAO calculations on the reference compound, i.e., tetramethylsilane (TMS), at the same IEFPCM-B3LYP/6-311++G(d,p) level.

All of the electronic structure calculations were carried out using the Gaussian03 program on an IBM X-series Cluster (with 340 nodes or 1,360 processors) at the University of Kentucky Center for Computational Sciences, and on a 34-processors IBM Linux Cluster in our own laboratory.

3 Conclusion

Extensive first-principles electronic structure calculations have led to a determination of the stable molecular conformations and the corresponding relative free energies of the protonated and deprotonated states of indolizidine (−)-235B′ in the gas phase, in chloroform, and in aqueous solution. The ^{1}H and ^{13}C NMR chemical shifts calculated using the computationally determined dominant molecular conformation of the deprotonated state are all consistent with available experimental NMR spectra of (−)-235B′ in chloroform, which suggests that the computationally determined molecular conformations are reasonable.

The calculated NMR chemical shifts in comparison with available experimental NMR data also help one to better understand and analyze the experimental NMR spectra of (−)-235B′. In particular, the available experimental ^{1}H NMR spectra showed only one H atom with a chemical shift (3.23 or 3.25 ppm) between ∼2.1 and ∼4.8 ppm. This unique ^{1}H chemical shift was assigned to the H atom on C8a (see Fig. 1 for the structure numbering) in previously reported experimental studies. However, our calculated chemical shift of H-8a is only ∼1.55 ppm. Our computational results reveal that the two geminal H atoms on C3 experience distinctly different magnetic shielding and, thus, have remarkably different chemical shifts (i.e., 3.24 and 2.03 ppm). Hence, the chemical shift at 3.23 ppm (or 3.25 ppm in another experimental measurement) should be assigned to one of the geminal H atoms on C3, rather than the H atom on C8a. It has also been demonstrated that the difference in the chemical shift between the two geminal H atoms on C3 is critically dependent on the conformation of (−)-235B′, as the difference becomes negligible in some other high-energy conformations based on our calculated results. The finding of the remarkably different chemical shifts of these geminal H atoms in a certain molecular conformation may also be valuable in understanding and analyzing the NMR spectra of other structurally related ring-containing compounds.

In addition, the pK_a of (−)-235B′ in aqueous solution has been predicted to be ∼9.7. All of the computational results obtained in this study provide a solid basis for future comprehensive studies on the microscopic and phenomenological binding of various receptor proteins with the protonated and deprotonated species of this potent and selective open-channel blocker of $\alpha 4\beta 2$ nAChRs.

This study not only helps to understand the detailed structures and conformations of (−)-235B′ in solution, but also demonstrates how one can appropriately use computational modeling and spectroscopic analysis to address the structural and spectroscopic problems that cannot be addressed by experiments alone.

Acknowledgments The research was supported in part by the Kentucky Science and Engineering Foundation (grant KSEF-925-RDE-008) and the National Institutes of Health (grant U19DA017548). The authors also acknowledge the Center for Computational Sciences (CCS) at University of Kentucky for supercomputing time on the IBM X-series Cluster (with 340 nodes or 1,360 processors).

References

1. Schneider G, Baringhaus K-H (2008) Molecular design: concepts and applications. Wiley-Vch, Weinheim, p 16
2. Daly JW, Spande TF, Garraffo HM (2005) J Nat Prod 68:1556
3. Carroll FI (2004) Bioorg Med Chem Lett 14:1889
4. Bunnelle WH, Daanen JF, Ryther KB, Schrimpf MR, Dart MJ, Gelain A, Meyer MD, Frost JM, Anderson DJ, Buckley M, Curzon P, Cao YJ, Puttfarcken P, Searle X, Ji J, Putman CB, Surowy C, Toma L, Barlocco D (2007) J Med Chem 50:3627
5. Michael JP (2007) Beilstein J Org Chem 3:27
6. Michel P, Rassat A, Daly JW, Spande TF (2000) J Org Chem 65:8908
7. Barluenga J, Mateos C, Aznar F, Valdes C (2002) Org Lett 4:1971
8. Marsden SP, McElhinney AD (2008) Beilstein J Org Chem 4:8
9. Toyooka N, Tsuneki H, Kobayashi S, Dejun Z, Kawasaki M, Kimura I, Sasaoka T, Nemoto H (2007) Curr Chem Biol 1:97
10. Tsuneki H, You Y, Toyooka N, Kagawa S, Kobayashi S, Sasaoka T, Nemoto H, Kimura I, Dani JA (2004) Mol Pharmacol 66:1061
11. Edwards MW, Daly JW (1988) J Nat Prod 51:1188
12. Wonnacott S, Sidhpura N, Balfour DJK (2005) Curr Opin Pharmacol 5:53
13. Karlin A (2002) Nat Rev Neurosci 3:102
14. Miyazawa A, Fujiyoshi Y, Unwin N (2003) Nature 423:949
15. Karlin A (2004) Neuron 41:841
16. Lester HA, Dibas MI, Dahan DS, Leite JF, Dougherty DA (2004) Trends Neurosci 27:329
17. Kihara T, Shimohama S (2004) Acta Neurobiol Exp 64:99
18. Schmaljohann J, Gündisch D, Minnerop M, Bucerius J, Joe A, Reinhardt M, Guhlke S, Biersack H, Wüllner U (2006) Nuclear Med Biol 33:305
19. Arneric SP, Holladay M, Williams M (2007) Biochem Pharmacol 74:1092
20. Tutka P (2008) Expert Opin Investig Drugs 17:1473
21. Zheng F, Zheng G, Deaciuc AG, Zhan C-G, Dwoskin LP, Crooks PA (2009) J Enzym Inhib Med Chem 24:157
22. Zheng F, Bayram E, Sumithran SP, Ayers JT, Zhan C-G, Schmitt JD, Dwoskin LD, Crooks PA (2006) Bioorg Med Chem 14:3017
23. Tonder JE, Olesen PH (2001) Curr Med Chem 8:651
24. Jensen AA, Frølund B, Liljefors T, Krogsgaard-Larsen P (2005) J Med Chem 48:4705
25. Huang X, Zheng F, Crooks PA, Dwoskin LP, Zhan C-G (2005) J Am Chem Soc 127:14401
26. Huang X, Zheng F, Chen X, Crooks PA, Dwoskin LP, Zhan C-G (2006) J Med Chem 49:7661
27. Huang X, Zheng F, Stokes C, Papke RL, Zhan C-G (2008) J Med Chem 51:6293
28. Huang X, Zheng F, Zhan C-G (2008) J Am Chem Soc 130:16691
29. Witala KW, Cramer CJ, Hoye TR (2007) Magn Reson Chem 45:819
30. Toyooka N, Tanaka K, Momose T (1997) Tetrahedron 53:9553
31. Collins I, Fox ME, Holmes AB, Williams SF, Baker R, Forbes IJ, Thompson M (1991) J Chem Soc Perkin Trans 1:175
32. Meijias JA, Lago S (2000) J Chem Phys 113:7306
33. Zhan C-G, Dixon DA (2001) J Phys Chem A 105:11534

34. Becke AD (1993) J Chem Phys 98:5648
35. Lee C, Yang W, Parr RG (1988) Phys Rev B 37:785
36. Stephens PJ, Devlin FJ, Chabalowski CF, Frisch MJ (1994) J Phys Chem 98:11623
37. Hehre WJ, Radom L, Schleyer PVR, Pople JA (1987) Ab initio molecular orbital theory. Wiley and Sons, New York
38. Florian J, Warshel A (1998) J Phys Chem B 102:719
39. Zhan C-G, Bentley J, Chipman DM (1998) J Chem Phys 108:177
40. Zhan C-G, Chipman DM (1998) J Chem Phys 109:10543
41. Zhan C-G, Chipman DM (1999) J Chem Phys 110:1611
42. Zhan C-G, Landry DW, Ornstein RL (2000) J Phys Chem A 104:7672
43. Zhan C-G, Niu S, Ornstein RL (2001) J Chem Soc Perkin Trans 2 1:23
44. Dixon DA, Feller D, Zhan C-G, Francisco JS (2002) J Phys Chem A 106:3191
45. Zheng F, Zhan C-G, Ornstein RL (2002) J Phys Chem B 106:717
46. Zhan C-G, Dixon DA (2002) J Phys Chem A 106:9737
47. Zhan C-G, Dixon DA, Sabri MI, Kim M-S, Spencer PS (2002) J Am Chem Soc 124:2744
48. Zhan C-G, Dixon DA (2003) J Phys Chem A 107:4403
49. Zhan C-G, Dixon DA, Spencer PS (2003) J Phys Chem B 107:2853
50. Dixon DA, Feller D, Zhan C-G, Francisco SF (2003) Int J Mass Spectrom 227:421
51. Lu H-T, Chen X, Zhan C-G (2007) J Phys Chem B 111:10599
52. Xiong Y, Zhan C-G (2006) J Phys Chem A 110:12644
53. Zhan C-G, Deng S-X, Skiba JG, Hayes BA, Tschampel SM, Shields GC, Landry DW (2005) J Comput Chem 26:980
54. Xiong Y, Zhan C-G (2004) J Org Chem 69:8451
55. Chen X, Zhan C-G (2004) J Phys Chem A 108:3789
56. Zhan C-G, Dixon DA (2004) J Phys Chem A 108:2020
57. Schmidt MW, Baldridge KK, Boatz JA, Elbert ST, Gordon MS, Jensen JH, Koseki S, Matsunaga N, Nguyen KA, Su SJ, Windus TL, Dupuis M, Montgomery JA (1993) J Comput Chem 14:1347
58. Vilkas MJ, Zhan C-G (2008) J Chem Phys 129:194109
59. Frisch MJ, Trucks GW, Schlegel HB, Scuseria GE, Robb MA, Cheeseman JR, Montgomery JA Jr, Vreven T, Kudin KN, Burant JC, Millam JM, Iyengar SS, Tomasi J, Barone V, Mennucci B, Cossi M, Scalmani G, Rega N, Petersson GA, Nakatsuji H, Hada M, Ehara M, Toyota K, Fukuda R, Hasegawa J, Ishida M, Nakajima T, Honda Y, Kitao O, Nakai H, Klene M, Li X, Knox JE, Hratchian HP, Cross JB, Adamo C, Jaramillo J, Gomperts R, Stratmann RE, Yazyev O, Austin AJ, Cammi R, Pomelli C, Ochterski JW, Ayala PY, Morokuma K, Voth GA, Salvador P, Dannenberg JJ, Zakrzewski VG, Dapprich S, Daniels AD, Strain MC, Farkas O, Malick DK, Rabuck AD, Raghavachari K, Foresman JB, Ortiz JV, Cui Q, Baboul AG, Clifford S, Cioslowski J, Stefanov BB, Liu G, Liashenko A, Piskorz P, Komaromi I, Martin RL, Fox DJ, Keith T, Al-Laham MA, Peng CY, Nanayakkara A, Challacombe M, Gill PMW, Johnson B, Chen W, Wong MW, Gonzalez C, Pople JA (2003) Gaussian 03, Revision A.1; Gaussian, Inc., Pittsburgh, PA
60. Chen X, Zhan C-G (2004) J Phys Chem A 108:6407
61. Zhan C-G, Landry DW, Ornstein RL (2000) J Am Chem Soc 122:2621
62. McWeeny R (1962) Phys Rev 126:1028
63. Ditchfield R (1974) Mol Phys 27:789
64. Dodds JL, McWeeny R, Sadlej AJ (1980) Mol Phys 41:1419
65. Wolinski K, Hilton JF, Pulay P (1990) J Am Chem Soc 112:8251
66. Cances E, Mennucci B, Tomasi J (1997) J Chem Phys 107:3032
67. Mennucci B, Cances E, Tomasi J (1997) J Phys Chem B 101:10506
68. Cances E, Mennucci B (1998) J Chem Phys 109:249
69. Cances E, Mennucci B (1998) J Math Chem 23:309
70. Cances E, Mennucci B, Tomasi J (1998) J Chem Phys 109:260
71. Tomasi J, Mennucci B, Cances E (1999) J Mol Struct Theochem 464:211
72. Amovilli C, Barone V, Cammi R, Cances E, Mennucci B, Pomelli C, Tomasi J (1999) Adv Quantum Chem 32:227